Front. Phys. 10(5), 106101 (2015)
DOI 10.1007/s11467-015-0504-y

RESEARCH ARTICLE

Role of confinement in water solidification under electric fields

Guo-Xi Nie[1], **Yu Wang**[2,*], **Ji-Ping Huang**[3,†]

[1] *Department of Physics, State Key Laboratory of Surface Physics, and Collaborative Innovation Center of Advanced Microstructures, Fudan University, Shanghai 200433, China*

[2] *Department of Physics, Zhejiang Agriculture and Forestry University, Hangzhou 311300, China*

[3] *Department of Physics, State Key Laboratory of Surface Physics, and Collaborative Innovation Center of Advanced Microstructures, Fudan University, Shanghai 200433, China*

*Corresponding authors. E-mail: *yuwang_zafu@126.com, †jphuang@fudan.edu.cn*

Received July 15, 2015; accepted September 16, 2015

In contrast to the common belief that confinement promotes water solidification, here we show by molecular dynamics simulations that confinement can impede water solidification under electric fields. The behavior is evidenced by the increase in critical electric field strength for water solidification as the confinement progresses. We also show that the solidification occurs more easily with a parallel field than a perpendicular one. We understand and generalize these results by developing an energy theory incorporated with the anisotropic Clausius–Mossotti equation. It is revealed that the underlying mechanism lies in the confinement effect on molecules' electro-orientations. Thus, it becomes possible to achieve electro-freezing (i.e., room-temperature ice) by choosing both confinement and electric fields appropriately.

Keywords molecular dynamics simulations, water, electric fields, confinement

PACS numbers 61.20.Ja, 81.30.Fb, 61.30.Hn, 64.70.Nd

1 Introduction

Owing to the importance of water, it has attracted much attention from scientists in various fields ranging across physics, chemistry, biology, and ecology. For water, a most important topic to scientists is phase transitions [1–22]. In particular, studies on water solidification are fundamentally crucial in environmental science (i.e., anticing materials [23, 24]) and biological techniques (e.g., fresh keeping [25] or effectiveness testing of antifreeze protein [26]). Molecular water thin films under confinement are the starting stage for the nucleation of ice around certain proteins [27]. Additionally, controlling the crystallization in cells is of great value in determining the ability of many organisms such as polar fish, bacteria, and plants to survive and thrive in subfreezing habitats [28].

It is known that the normal freezing temperature is 0 °C for bulk liquid water. Hence, for potential applications, how to raise the freezing temperature becomes a challenge. On one hand, confinement has frequently been suggested in the literature [6–10, 29–33]. For example, researchers [6–10, 29–33] have reported that extreme confinement can promote the spontaneous solidification of water or other liquids, which results from the reduction of entropy due to confinement. For example, a monolayer of ice at 300 K in a confined system has been reported [7]. Actually, when water is thinner than 4–6 molecular layers, solidification can be promoted by confinement [6–10]. On the other hand, some researchers have suggested the use of electric fields together with confinement [12, 13, 17–20]. This is because electric fields can provide the activation energy for nucleation by inducing the rearrangement of hydrogen-bond networks through the torsion of water molecules. The synthetical effect from electric fields and confinement induces novel phenomena and a better understanding of water solidification. Lateral electric fields were employed by Qian *et al.* [34] on confined water within a fixed separation between two walls, and three kinds of bilayer ice were found at 230 K as the electric field was increased to specific values. Zhu *et al.* [35] investigated phase transitions of the first water layer adsorbed onto charged graphene at room temperature from electromelting to electrofreezing as the charge value increased, which is attributed to the change of water–water interactions from attractive to repulsive at a critical charge value. Mei *et al.* [36] explored the phase behavior of water confined between two solid walls, where positive and negative charges of the same magni-

tude were assigned to atoms located diagonally in neighboring hexagons. A transition between two kinds of ice was found at 240 K as surface charges were increased, and their formation was due to nanoconfinement and surface charges, respectively. Simulations [12, 13, 17, 19] and experiments [20] have helped to reveal that water between nanogaps can freeze into a solid phase with a higher freezing temperature when external electric fields are added parallel [17] or perpendicular [12, 13, 19, 20] to the two walls forming the nanogap. In other words, when the degree of confinement is fixed, the addition of external electric fields can raise the freezing temperature as expected, and a stronger field yields a higher freezing temperature due to the input of more activation energy for nucleation. However, the inverse question has never been asked. That is, when the external electric field is fixed and added to a nanogap containing water molecules with a constant number density, can an increasing degree of confinement help to raise the freezing temperature? (The reason why we specify "a constant number density" herein is that we need to focus on the pure effect of confinement by fixing the initial state of water.) Evidently, asking such an inverse question is necessary because of its academic significance and practical importance. Clearly, an intuitive answer to this question might be "YES" but our answer is "NO," which is counterintuitive indeed. To achieve our answer to the question, we resort to full-atom molecular dynamics simulations, together with an independent energy theory incorporated with the anisotropic Clausius–Mossotti equation. As a result, we found that parallel electric fields are more favorable for water solidification than perpendicular electric fields. Now let us proceed by first introducing the molecular dynamics simulations.

2 Molecular dynamics simulations: Methods and results

2.1 Methods

Molecular dynamics simulation, which has been widely used for studies of water dynamics [7, 18, 19, 37–41], is adopted here. Figure 1(a) displays our simulation system containing water molecules between two parallel graphite sheets, each having an area of 4.762 nm×5.006 nm within the XY plane. The distance (d) between the two sheets ranged from 1.2 to 4.4 nm, and the simulation data were collected every 0.2 nm. It is worth mentioning that the specific range of d contained the confined systems that corresponded to water films thinner than 4–6 molecular layers [42]. Note that a water film that has a thickness larger than 7–8 molecular layers behaves as bulk water rather than confined water [42]. In our simulations, external electric fields (E) were applied along the Z or X axes and are called perpendicular or parallel electric fields accordingly. The electric field strength (E) ranged from 0 to 50 V/nm, as was adopted in previous simulations [12–14, 16, 18, 19]. In addition, according to Refs. [29–33], where the influence of confinement on liquids for field-free systems has been investigated through experiments and simulations, we also kept the number density of water molecules as a constant, 30.2 nm^{-3}, for all our simulations in order to focus on the pure effect of confinement on electro-freezing by fixing the initial state of water molecules [14, 17, 43].

More details on simulations are introduced as follows. We chose a canonical ensemble at room temperature (300 K) by resorting to the molecular dynamics package Gromacs 4.0.7 [44, 45]. Water molecules were modeled with the extended simple point charge (SPC/E) pair potential [46], and the water–wall interactions were treated by the Lennard–Jones potential, $V_{LJ} = 4\varepsilon[(\frac{\sigma}{r})^{12} - (\frac{\sigma}{r})^{6}]$, where ε and σ come from Ref. [47]. The particle-mesh Ewald method [48] was used for the electrostatic interaction; evaluation of non-bonded interactions was performed by using a twin range cutoff of 0.9 nm and 1.4 nm for the Coulombic and Lennard–Jones potentials, respectively. We also adopted the thermostat of Nosé and Hoover [49–51] with a time constant of 0.5 ps. Moreover, the periodic boundary condition was used along the X and Y directions. To avoid non-physical results, we set the size of the simulation box along the Z direction to be three times the distance between the two sheets, which is similar to the EW3DC method [52]. In our simulations, a time step of 2 fs was adopted. The simulation for each parameter set ran for 5 ns, and the last 3 ns were collected for analysis. Additionally, we considered two water molecules to form a hydrogen bond if the distance O...O is shorter than 0.35 nm and simultaneously the angle O-H...O is less than 30°.

2.2 Results and discussion

Figure 1(b) displays snapshots of the water structure in a liquid phase without E and two solid phases with E for $d = 1.4$ nm. It is evident that cubic [12, 13] and hexagonal ice [17] were formed under the perpendicular and parallel fields, respectively. In addition, if d increases up to a value larger than 7–8 molecular layers, we confirmed that the water structures in both the perpendicular and parallel field cases were cubic ice.

Figure 2 shows the lateral diffusion coefficients of the XY coordinate plane as a function of electric field strength for systems with different d values in the

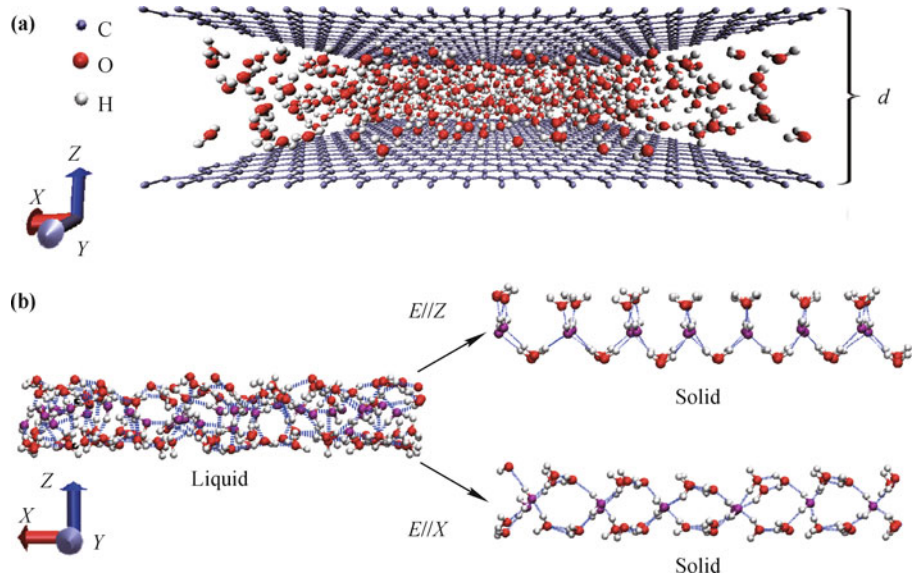

Fig. 1 **(a)** A perspective view of our simulation system with water molecules confined between two parallel graphite sheets within the XY plane. The distance between the two sheets is denoted by d; the three different atoms, H (hydrogen), O (oxygen), and C (carbon), are indicated. **(b)** Snapshots of water structure in a liquid phase (without electric field E) and two solid phases (with E), where oxygen atoms in different sublayers are indicated by different colors (red and purple). For a perpendicular (or parallel) electric field $E = 50\,\mathrm{V/nm}$ (or $20\,\mathrm{V/nm}$) along the Z (or X) axis, cubic ice (or hexagonal ice) is formed.

presence of perpendicular or parallel electric fields. For clarity, we focus on the critical electric field (E_c), at which point the lateral diffusion coefficients abruptly decrease as E increases. According to the meaning of the lateral diffusion coefficients, we are allowed to consider the water to behave as a solid or liquid for $E > E_c$ or $E < E_c$. Under a perpendicular field, as d=1.2 nm, E_c is approximately 38 V/nm. With increasing d, E_c suddenly decreases to ∼15 V/nm as d >2.4 nm. Some of these results agree with previous reports. For example, at room temperature, when d is approximately 1.8 nm, the critical field strength is approximately 30 V/nm [16], and it is between 10–20 V/nm when d=4.0 nm [13]. However, for the parallel electric field, it only changes from 9 V/nm to 5 V/nm with increasing d. Here, the partial results also agree with the previous work [17].

From the two insets of Fig. 2, we find that E_c increases as d decreases, which indicates that a stronger degree of confinement makes water solidification more difficult. On the other hand, we also find that at a given value of d, the E_c values for parallel field cases [Fig. 2(b)] are always smaller than those for perpendicular field cases [Fig. 2(a)]. This indicates that parallel electric fields are more favorable for water solidification than perpendicular electric fields.

In order to understand the results obtained from Fig. 2, we further analyzed the simulation data, with a focus on the radial distribution function of water molecules, average components of the dipole moment per water molecule, and the average number of hydrogen bonds per water molecule. Radial distribution functions (RDFs) can be used to analyze the structure of water. Liquid and solid water display different structural features in the RDF. In particular, liquid water has platforms or low-resolution-peaks in the RDF, whereas solid water or water with a crystal-like structure has spiculate peaks. The results are shown in Fig. 3. Under perpendicular electric fields ($E_\perp$) [Fig. 3(a)], as d=1.2 nm, where $E_c \approx 38\,\mathrm{V/nm}$, water exhibits a crystal-like structure when $E_\perp$ =40 V/nm, and it remains liquid when $E_\perp < E_c$; as d=1.8 nm, where $E_c \approx 26\,\mathrm{V/nm}$, a crystal-like structure is found in both cases with $E_\perp$=30 V/nm and 40 V/nm; when d=3.0 nm, the crystal-like structures also occur when $E_\perp$ is larger than the critical electric field E_c ≈18 V/nm. On the other hand, Fig. 3(b) shows the RDFs for parallel electric fields ($E_{//}$). The results also depend on the shift of E_c values, which echoes the results shown in Fig. 3(a). Comparing Fig. 3(a) and Fig. 3(b), we find that for a small d of 1.2 nm, cubic ice and hexagonal ice are observed for the perpendicular and parallel electric fields, respectively. However, in a bulk-like case (such as d=3.0 nm), crystal-like structures in both systems appear to be cubic. Figure 3(c) shows a further comparison. As d increases, the degree of overlapping of RDFs for both systems shows the tendency to be the same cubic structure.

When water freezes, water molecules align in an ordered manner through the rearrangement of water dipoles. First, to reveal the mechanism of water orientation for field-free systems, the absolute average molec-

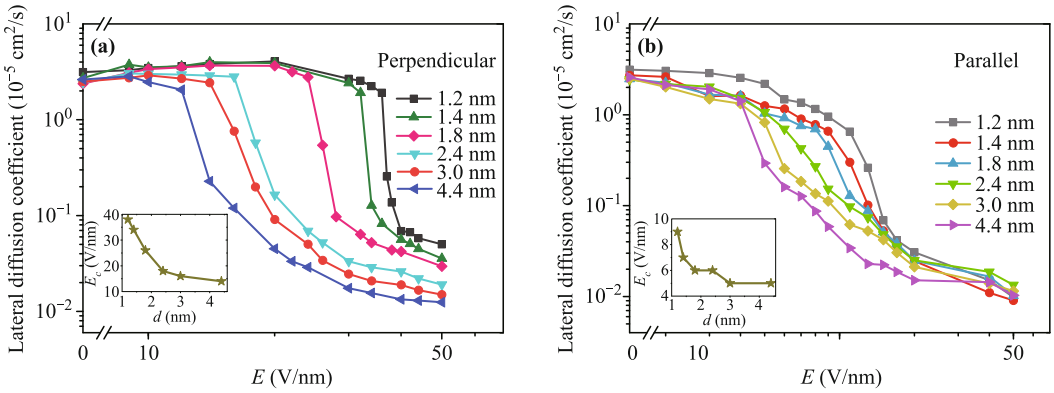

Fig. 2 Lateral diffusion coefficients as a function of electric field strengths (E) for confined systems with different d values in the presence of **(a)** a perpendicular electric field and **(b)** a parallel electric field; d = 1.2, 1.4, 1.8, 2.4, 3.0, and 4.4 nm. The two insets in (a) and (b) show that the critical field strength, E_c, increases as d decreases. Note that the scales of E are different in (a) and (b).

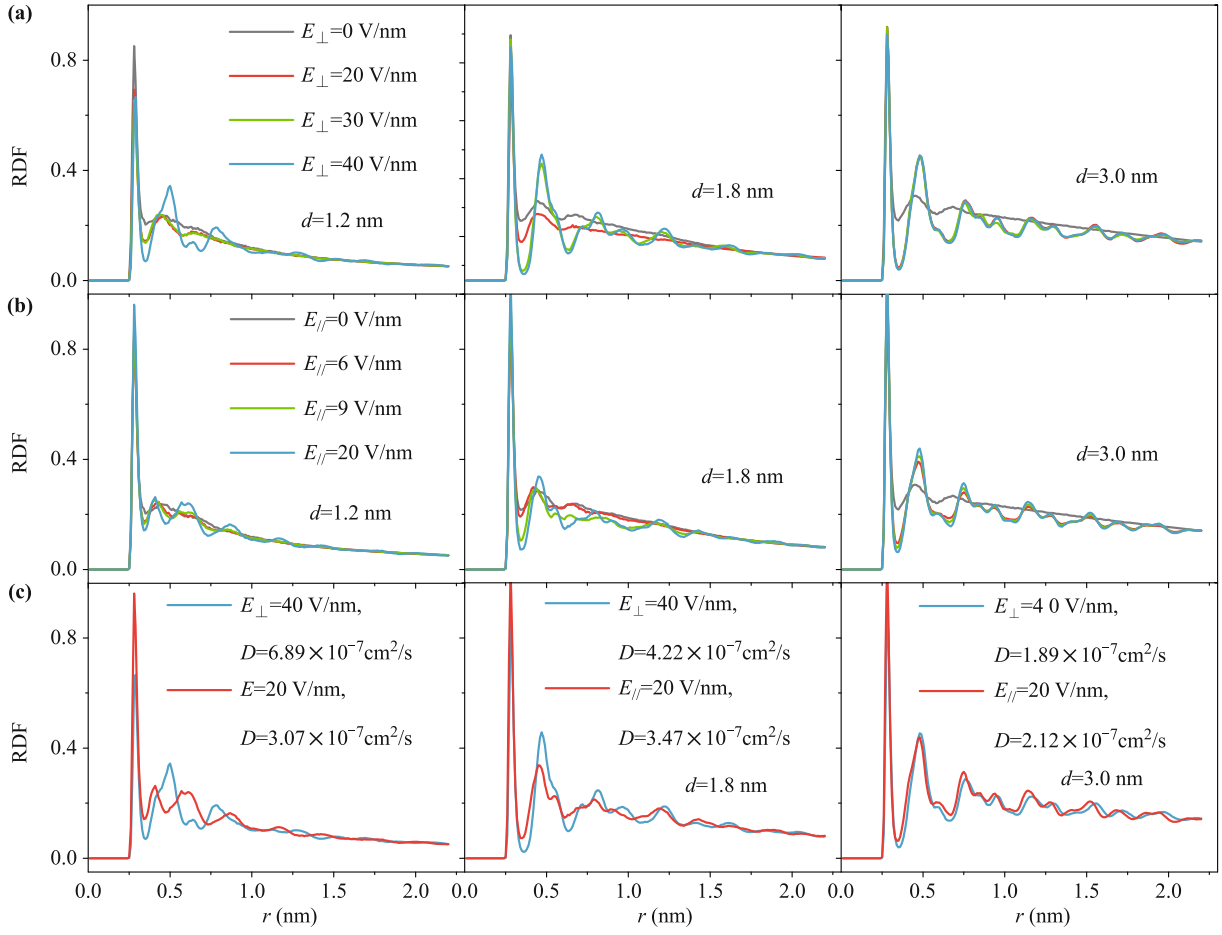

Fig. 3 Radial distribution function (RDF) of water molecules for d=1.2, 1.8, and 3.0 nm **(a)** under perpendicular electric fields ($E_\perp$) of 0, 20, 30, and 40 V/nm and **(b)** parallel electric fields ($E_{//}$) of 0, 6, 9, and 20 V/nm. **(c)** Comparison between the RDFs for the two systems with $E_\perp$ = 40 V/nm and $E_{//}$ =20 V/nm. The two systems have close lateral diffusion coefficients (D).

ular dipole moments (P) along the X, Y, and Z directions (P_X, P_Y, and P_Z) are calculated respectively. $P_n = (\sum_{i=1}^{N} |p_{in}|)/N$, $n = X, Y, Z$, where p is the dipole moment of each water molecule and N is the number of water molecules in each system. It should be noticed that P_X, P_Y, and P_Z exclude the offset of dipole moments along inverse directions in order to present the dipolar orientation preference among the three axes. The results are shown in Fig. 4(a). P_X and P_Y, which are parallel to the walls, are almost same, but they are larger than

P_Z. This is because the walls break the hydrogen bonds along the Z direction. Additionally, as d increases, water tends to be isotropic since the three components along the X, Y, and Z directions tend to be close to each other. If we add an external electric field, the structure of water should be changed due to the reorientation of water dipoles, thus yielding new structures. In Fig. 4(b), as the perpendicular electric field E increases, P_Z gradually exceeds P_X and P_Y. Moreover, the smaller d is, the more difficult P_X and P_Y are overstepped by P_Z. Under a parallel electric field E, P_X increases fast, whereas P_Y and P_Z decrease and become close to each other. These results are shown in Fig. 4(c).

On the other hand, to find the degree of molecular dipoles' uniform orientation under various E values in each system, we calculated the average molecular dipole moments along the Z (Q_Z) or X (Q_X) direction as a function of perpendicular or parallel electric fields for different d values according to $Q_k = (\sum_{i=1}^{N} p_{ik})/N$, where

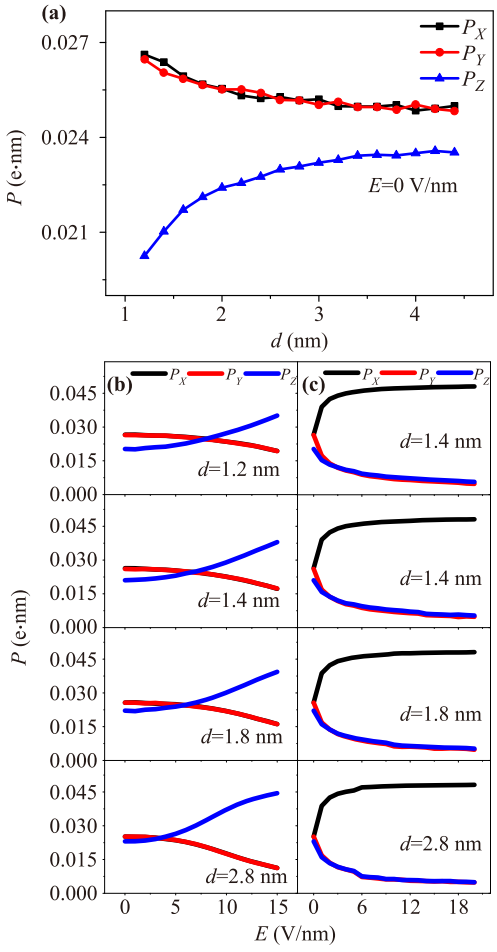

Fig. 4 Average components of the dipole moment per water molecule in absolute value along the X, Y, and Z directions as a function of **(a)** d for $E = 0\,\mathrm{V/nm}$, **(b)** perpendicular field strength for various d values, and **(c)** parallel field strength for various d values. Note that the black and red curves in (b) are overlapped.

$k = X, Z$; see Fig. 5. Note that Q_Z and Q_X include the offset of molecular dipole moments along the inverse directions. It is obvious that with increasing E, the average molecular dipole moments in all systems increase and then converge. This implies that as E strengthens, the consistent degree of dipolar orientation increases and reaches a threshold after E reaches specific values. However, such a consistent degree of dipolar orientation under parallel electric fields occurs more easily than those with perpendicular ones because weaker electric fields are required. Moreover, water dipoles at smaller d values are rotated more laboriously than those at larger d values for the same perpendicular or parallel electric field strength. In general, Fig. 5 shows that the more a confined system impedes the molecular structure being rearranged, the stronger E_c is needed. This helps to understand Fig. 2.

Another important step for water solidification is the rebuilding of the hydrogen-bond network. Therefore, the average number of hydrogen bonds per water molecule under different field strengths for systems with perpendicular or parallel electric fields was calculated, and the results are graphed in Fig. 6. Generally, in each system, as E increases, the number of hydrogen bonds initially decreases; it then increases and converges. Here, the electric field at which the number of hydrogen bonds starts to increase corresponds to the critical electric field adopted in the main text. When the electric field E is relatively small ($E < E_c$), it helps to rotate water dipoles, breaking the original hydrogen-bond network. However, it is not strong enough to rebuild a new network, so the number of hydrogen bonds decreases. When the electric field increases further, a new hydrogen-bond network is established gradually, and the solidification of water begins to appear.

In general, the underlying mechanism lies in the fact that water dipoles prefer to be parallel to walls without E. Owing to this preference of orientation, for field-free systems, a strong degree of confinement can promote an orderly alignment of molecular dipoles, thus helping solidification to occur. However, when an external electric field is applied, water dipoles tend to be directed along the direction of E. Furthermore, in the case of a stronger degree of confinement, it becomes more difficult to rotate water dipoles, which causes the inverse correlation between E_c and d observed in Fig. 2.

Accordingly, since water dipoles tend to be parallel to walls without E, it requires more energy for the perpendicular electric field than for the parallel electric field to make solidification occur. Thus, parallel electric fields are more favorable for water solidification than perpendicular electric fields. Such analysis is consistent and can be used to explain Fig. 2. However, this analysis is based

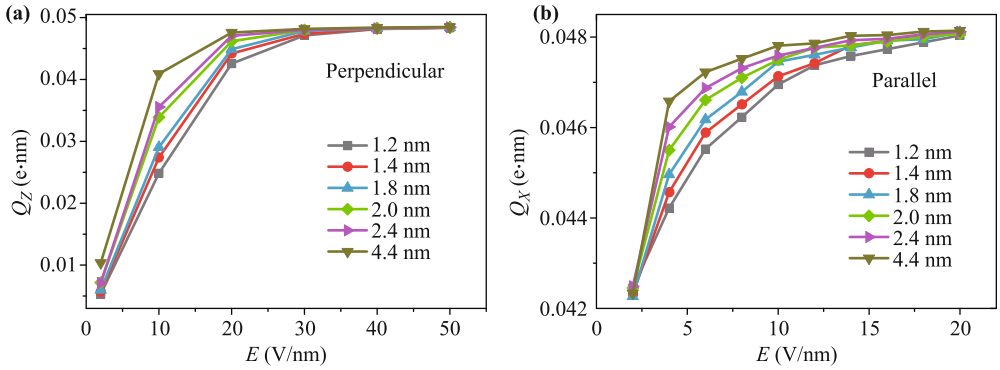

Fig. 5 **(a)** Average Z-directed component of the dipole moment per water molecule, Q_Z, for d = 1.2–4.4 nm versus perpendicular electric fields (along the Z axis); **(b)** Average X-directed component of the dipole moment per water molecule, Q_X, for d = 1.2–4.4 nm versus parallel electric fields (along the X axis). Note that the range of electric fields is different in (a) and (b).

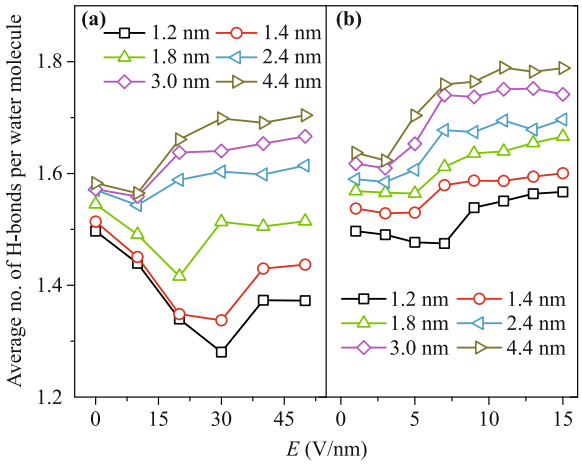

Fig. 6 Average number of hydrogen bonds per water molecule as a function of **(a)** perpendicular electric fields (0–50 V/nm) and **(b)** parallel electric fields (1–15 V/nm).

on the simulation data only. Thus, we are in a position to develop an independent energy theory for understanding and generalizing the above simulation results. Here the wording "generalizing" means that the theory presented below is independent of both the specific water model and the specific graphite sheets that were adopted for conducting the above simulations.

3 Energy theory incorporated with the anisotropic Clausius–Mossotti equation: Comparison with simulation results

According to the above simulations, we have drawn two key conclusions: one is that confinement can impede water solidification in the presence of an external electric field; the other is that water solidification occurs more easily with a parallel electric field than with a perpendicular one. In the preceding section, in order to understand the two conclusions, we have analyzed the simulation data by plotting Figs. 3–6. Nevertheless, in order to understand and generalize the simulation results, we feel obligated to develop an independent theory as follows.

Let us start by considering the electrostatic energy density, namely, the volume-averaged electrostatic energy (U) for the whole confined system in the presence of an external electric field E,

$$U = \frac{1}{2}\varepsilon_w E^2, \tag{1}$$

where ε_w is the effective dielectric constant of water molecules confined between the two walls. On the other hand, the electrostatic energy density (U_v) for the same system without water molecules is given by

$$U_v = \frac{1}{2}\varepsilon_v E^2, \tag{2}$$

where ε_v is the dielectric constant of a vacuum. Clearly, the difference between U and U_v, $\Delta U = U - U_v$, represents the volume-averaged electrostatic energy stored by the water molecules only.

$$\Delta U = \frac{1}{2}(\varepsilon_w - \varepsilon_v)E^2. \tag{3}$$

The substitution of $E = 0$ V/nm into Eq. (3) yields $\Delta U = 0$, which corresponds to the fact that the water molecules are distributed randomly due to the lack of external electric field. On the other hand, when $E \neq 0$ V/nm, Eq. (3) leads to $\Delta U \neq 0$, indicating that the water molecules tend to be directed along the direction of E and become closer. This process is just the signal of solidification resulting from the input of electrostatic energy. In other words, the solidification of water molecules is equivalent to the process of storing the electrostatic energy in the water molecules. Namely, larger ΔU causes a higher degree of solidification of water molecules in the

confined system. Next, in order to calculate ΔU in Eq. (3), we must first determine the term, $\varepsilon_w - \varepsilon_v$. For this purpose, we resort to the anisotropic Clausius–Mossotti equation [53–55].

$$\frac{g_L(\varepsilon_w - \varepsilon_v)}{\varepsilon_v + g_L(\varepsilon_w - \varepsilon_v)} = \frac{4\pi}{3} N_1 \left(\alpha + \frac{p^2}{3k_{\mathrm{B}}T}\right), \tag{4}$$

where N_1 is the number density of water molecules, which is constant for different systems with different d values throughout this work, α the polarizability, p the permanent electric dipole moment of a water molecule, k_B the Boltzmann constant, and T the absolute temperature. In Eq. (4), g_L is the local field factor [56–58], which is used to measure the degree of structural anisotropy resulting from the formation of molecular chains caused by the external electric field E. Within the chain, the permanent dipole moment of each water molecule tends to be directed along the direction of E, as required by the interaction between the dipole moment and E. g_L can be given by [56, 57]

$$g_L = \frac{1}{1-\rho^2} + \frac{\rho}{(\rho^2-1)^{3/2}} \ln(\rho + \sqrt{\rho^2 - 1}). \tag{5}$$

Here $\rho(>1)$ is the ratio between the averaged length (l) of water chains and the diameter of a water molecule ($d_w = 0.4\,\mathrm{nm}$). In particular, $\rho = 1$ corresponds to $g_L = 1/3$, an isotropic case where water molecules are randomly distributed due to the lack of external electric field ($E = 0\,\mathrm{V/nm}$). Because the chain cannot be perfectly straight and the water molecules cannot be perfectly touching within the chain (due to thermal motion), the value of ρ could be a non-integer, satisfying $\rho \geqslant 1$. For the perpendicular field case, water chains are along the Z axis and $l \approx d$. According to the definition of ρ, we may estimate ρ by using $\rho = d/d_w$ for different d values. For example, $d = 4.4$ nm yields $\rho = 11$ in Fig. 7. For the parallel field case, water chains are along the X axis. To achieve qualitative results, the actual value of ρ is not necessary, but ρ must satisfy three requirements: (i) Because our system is confined along the Z axis but open along the X and Y axes, $l \gg d$. Then, the lowest value of ρ must be larger than the maximum value obtained for the perpendicular field case, 11; (ii) The confinement impedes the reorientation of water dipoles induced by electric fields, so with a smaller d, the confinement is stronger and tends to break the field-directed water chains. Thus, ρ will increase as d becomes larger; (iii) It will not increase as much as that in the perpendicular case because the number density of water molecules is constant in our systems. To qualitatively understand the simulation results, we assume that ρ increases from 12 to 14 as d increases from 1.2 nm to 4.4 nm in Fig. 7.

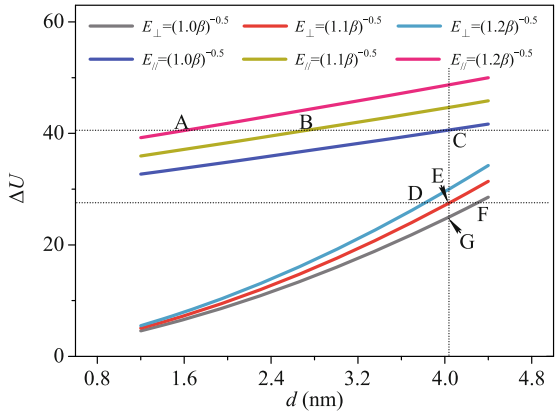

Fig. 7 ΔU as a function of d for the confined systems under perpendicular electric fields ($E_\perp$) or parallel electric fields ($E_{//}$), which is calculated according to Eq. (7). Two horizontal dashed lines and one vertical dashed line are indicated for comparison. Points A–G represent the intersection points.

According to Eq. (4), we obtain

$$\varepsilon_w - \varepsilon_v = \frac{\frac{4\pi}{3} N_1 (\alpha + \frac{p^2}{3k_B T})\varepsilon_v}{[1 - \frac{4\pi}{3} N_1 (\alpha + \frac{p^2}{3k_B T})] g_L} \equiv \frac{\beta}{g_L}. \tag{6}$$

Here, β denotes a positive constant. By substituting Eq. (6) into Eq. (3), we obtain

$$\Delta U = \frac{1}{2} \frac{\beta}{g_L} E^2. \tag{7}$$

Based on Eq. (7), we performed numerical calculations; see Fig. 7, which shows the effect of different electric fields on ΔU for both perpendicular and parallel field cases. It is evident that ΔU decreases as d decreases in both cases. That is, for a smaller d, namely, a higher degree of confinement, the volume-averaged electrostatic energy stored by water molecules is smaller. In particular, for parallel field cases, points A–C represent three systems with increasing d but decreasing E in order, which, however, correspond to the same ΔU. They show that a stronger external field strength is needed for a narrower space to reach the same electrostatic energy (i.e., the same degree of solidification). The behavior also holds for perpendicular field systems (see points D–F). This fact shows that the confinement can impede solidification under specific external electric fields. On the other hand, comparing points C and G, we find that with the same E and d, the system with a parallel external electric field has a higher electrostatic energy density, which results in easier solidification for parallel field systems than for perpendicular field systems.

So far, the two conclusions obtained from our molecular dynamics simulations have been well understood and generalized by using the energy theory based on the anisotropic Clausius–Mossotti equation.

4 Conclusions

We have performed full-atom molecular dynamics simulations for water molecules within the nano-gap formed by two graphite sheets at room temperature and have drawn the following conclusions. Confinement at the nano-scale can impede water solidification in the case of external electric fields; this result is in contrast to the common knowledge that confinement promotes water solidification. In addition, water solidification occurs more easily with a parallel electric field than with a perpendicular one.

The simulation results have been well understood and generalized by developing the energy theory based on the anisotropic Clausius–Mossotti equation. As revealed by us, the general mechanism originates from the effect of the confinement of the walls on the electro-orientations of the water molecules. Thus, it becomes possible to achieve various kinds of electro-freezing (such as room-temperature ice) or electro-melting by choosing confinement and electric fields appropriately.

Acknowledgements We acknowledge the financial support by the National Natural Science Foundation of China under Grant Nos. 11222544 and 11304284 (Y. Wang), the Fok Ying Tung Education Foundation under Grant No. 131008, the Program for New Century Excellent Talents in University (Grant No. NCET-12-0121), and the CNKBRSF under Grant No. 2011CB922004. The computational resources utilized in this research were provided by Shanghai Supercomputer Center.

References

1. A. Cupane, M. Fomina, I. Piazza, J. Peters, and G. Schiro, Experimental evidence for a liquid-liquid crossover in deeply cooled confined water, *Phys. Rev. Lett.* 113(21), 215701 (2014)
2. A. G. Marín, O. R. Enriquez, P. Brunet, P. Colinet, and J. H. Snoeijer, Universality of tip singularity formation in freezing water drops, *Phys. Rev. Lett.* 113(5), 054301 (2014)
3. Z. Wang, K. H. Liu, P. S. Le, M. D. Li, W. S. Chiang, J. B. Leão, J. R. D. Copley, M. Tyagi, A. Podlesnyak, A. I. Kolesnikov, C.Y. Mou, and S. H. Chen, Boson peak in deeply cooled confined water: A possible way to explore the existence of the liquid-to-liquid transition in water, *Phys. Rev. Lett.* 112(23), 237802 (2014)
4. W. J. Cho, J. Kim, J. Lee, T. Keyes, J. E. Straub, and K. S. Kim, Limit of metastability for liquid and vapor phases of water, *Phys. Rev. Lett.* 112(15), 157802 (2014)
5. K. Raghavan, K. Foster, K. Motakabbir, and M. Berkowitz, Structure and dynamics of water at the pt(111) interface: Molecular dynamics study, *J. Chem. Phys.* 94(3), 2110 (1991)
6. P. A. Thompson, G. S. Grest, and M. O. Robbins, Phase transitions and universal dynamics in confined films, *Phys. Rev. Lett.* 68(23), 3448 (1992)
7. R. Zangi and A. E. Mark, Monolayer ice, *Phys. Rev. Lett.* 91(2), 025502 (2003)
8. R. Zangi and A. E. Mark, Bilayer ice and alternate liquid phases of confined water, *J. Chem. Phys.* 119(3), 1694 (2003)
9. K. Koga and H. Tanaka, Phase diagram of water between hydrophobic surfaces, *J. Chem. Phys.* 122(10), 104711 (2005)
10. K. B. Jinesh and J. W. M. Frenken, Experimental evidence for ice formation at room temperature, *Phys. Rev. Lett.* 101(3), 036101 (2008)
11. I. M. Svishchev and P. G. Kusalik, Crystallization of liquid water in a molecular dynamics simulation, *Phys. Rev. Lett.* 73(7), 975 (1994)
12. X. Xia and M. L. Berkowitz, Electric-field induced restructuring of water at a platinum-water interface: A molecular dynamics computer simulation, *Phys. Rev. Lett.* 74(16), 3193 (1995)
13. X. Xia, L. Perera, U. Essmann, and M. L. Berkowitz, The structure of water at platinum/water interfaces molecular dynamics computer simulations, *Surf. Sci.* 335(1-3), 401 (1995)
14. I. M. Svishchev and P. G. Kusalik, Electrofreezing of liquid water: A microscopic perspective, *J. Am. Chem. Soc.* 118(3), 649 (1996)
15. I. Borzsák and P. T. Cummings, Electrofreezing of water in molecular dynamics simulation accelerated by oscillatory shear, *Phys. Rev. E* 56(6), R6279 (1997)
16. G. Sutmann, Structure formation and dynamics of water in strong external electric fields, *J. Electroanal. Chem.* 450(2), 289 (1998)
17. R. Zangi and A. E. Mark, Electrofreezing of confined water, *J. Chem. Phys.* 120(15), 7123 (2004)
18. X. Hu, N. Elghobashi-Meinhardt, D. Gembris, and J. C. Smith, Response of water to electric fields at temperatures below the glass transition: A molecular dynamics analysis, *J. Chem. Phys.* 135(13), 134507 (2011)
19. H. Qiu and W. L. Guo, Electromelting of confined monolayer ice, *Phys. Rev. Lett.* 110(19), 195701 (2013)
20. E. M. Choi, Y. H. Yoon, S. Lee, and H. Kang, Freezing transition of interfacial water at room temperature under electric fields, *Phys. Rev. Lett.* 95(8), 085701 (2005)
21. D. L. Scovell, T. D. Pinkerton, V. K. Medvedev, and E. M. Stuve, Phase transitions in vapordeposited water under the influence of high surface electric fields, *Surf. Sci.* 457(3), 365 (2000)
22. G. Chen, P. Tan, S. Chen, J. P. Huang, W. Wen, and L. Xu, Coalescence of pickering emulsion droplets induced by an electric field, *Phys. Rev. Lett.* 110(6), 064502 (2013)
23. P. Kim, T. S. Wong, J. Alvarenga, M. J. Kreder, W. E. Adorno-Martinez, and J. Aizenberg, Liquid-infused nanostructured surfaces with extreme anti-ice and anti-frost performance, *ACS Nano* 6(8), 6569 (2012)

24. M. Lee, C. Yim, and S. Jeon, Communication: Anti-icing characteristics of superhydrophobic surfaces investigated by quartz crystal microresonators, *J. Chem. Phys.* 142(4), 041102 (2015)
25. A. Loncaric, K. Dugalic, I. Mihaljevic, L. Jakobek, and V. Pilizota, Effects of sugar addition on total polyphenol content and antioxidant activity of frozen and freeze-dried apple puree, *J. Agric. Food Chem.* 62(7), 1674 (2014)
26. T. Inada, T. Koyama, F. Goto, and T. Seto, Ice nucleation in emulsified aqueous solutions of antifreeze protein type III and poly(vinyl alcohol), *J. Phys. Chem. B* 115(24), 7914 (2011)
27. D. Murakami and K. Yasuoka, Molecular dynamics simulation of quasi-two-dimensional water clusters on ice nucleation protein, *J. Chem. Phys.* 137(5), 054303 (2012)
28. K. Meister, S. Ebbinghaus, Y. Xu, J. G. Duman, A. DeVries, M. Gruebele, D. M. Leitner, and M. Havenith, Long-range protein-water dynamics in hyperactive insect antifreeze protein, *Proc. Natl. Acad. Sci. USA* 110(5), 1617 (2013)
29. P. A. Thompson and M. O. Robbins, Origin of stick-slip motion in boundary lubrication, *Science* 250(4982), 792 (1990)
30. M. O. Robbins and P. A. Thompson, Critical velocity of stick-slip motion, *Science* 253(5022), 916 (1991)
31. J. N. Israelachvili, P. M. McGuiggan, and A. M. Homola, Dynamic properties of molecularly thin liquid films, *Science* 240(4849), 189 (1988)
32. S. Granick, Motions and relaxations of confined liquids, *Science* 253(5026), 1374 (1991)
33. J. Klein and E. Kumacheva, Confinement-induced phase transitions in simple liquids, *Science* 269(5225), 816 (1995)
34. Z. Y. Qian and G. H. Wei, Electric-field-induced phase transition of confined water nanofilms between two graphene sheets, *J. Phys. Chem. A* 118(39), 8922 (2014)
35. X. Y. Zhu, Q. Z. Yuan, and Y. P. Zhao, Phase transitions of a water overlayer on charged graphene: from electromelting to electrofreezing, *Nanoscale* 6(10), 5432 (2014)
36. F. Mei, X. Y. Zhou, J. L. Kou, F. M. Wu, C. L. Wang, and H. J. Lu, A transition between bistable ice when coupling electric field and nanoconfinement, *J. Chem. Phys.* 142(13), 134704 (2015)
37. Y. S. Tu, P. Xiu, R. Z. Wan, J. Hu, R. H. Zhou, and H. P. Fang, Water-mediated signal multiplication with Y-shaped carbon nanotubes, *Proc. Natl. Acad. Sci. USA* 106(43), 18120 (2009)
38. Y. Wang, Y. J. Zhao, and J. P. Huang, Giant pumping of single-file water molecules in a carbon nanotube, *J. Phys. Chem. B* 115(45), 13275 (2011)
39. J. Y. Su and H. X. Guo, Control of unidirectional transport of single-file water molecules through carbon nanotubes in an electric field, *ACS Nano* 5(1), 351 (2011)
40. X. W. Meng and J. P. Huang, Enhanced permeation of single-file water molecules across a noncylindrical nanochannel, *Phys. Rev. E* 88(1), 014104 (2013)
41. Y. Wang and J. P. Huang, A water-based molecular flip-flop, *Eur. Phys. J. Appl. Phys.* 68(3), 30403 (2014)
42. R. Zangi, Water confined to a slab geometry: A review of recent computer simulation studies, *J. Phys.: Condens. Matter* 16(45), S5371 (2004)
43. N. Giovambattista, P. J. Rossky, and P. G. Debenedetti, Phase transitions induced by nanoconfinement in liquid water, *Phys. Rev. Lett.* 102(5), 050603 (2009)
44. B. Hess, C. Kutzner, D. van der Spoel, and E. Lindahl, GROMACS 4: Algorithms for highly efficient, load-balanced, and scalable molecular simulation, *J. Chem. Theory Comput.* 4(3), 435 (2008)
45. G. X. Guo, L. Zhang, and Y. Zhang, Molecular dynamics study of the infiltration of lipidwrapping C_{60} and polyhydroxylated single-walled nanotubes into lipid bilayers, *Front. Phys.* 10(2), 177 (2015)
46. H. J. C. Berendsen, J. R. Grigera, and T. P. Straatsma, The missing term in effective pair potentials, *J. Chem. Phys.* 91(24), 6269 (1987)
47. G. Hummer, J. C. Rasaiah, and J. P. Noworyta, Water conduction through the hydrophobic channel of a carbon nanotube, *Nature* 414(6860), 188 (2001)
48. T. A. Darden, D. M. York, and L. G. Pedersen, Particle mesh Ewald: An $N{\cdot}\log(N)$ method for Ewald sums in large systems, *J. Chem. Phys.* 98(12), 10089 (1993)
49. S. Nosé, A unified formulation of the constant temperature molecular dynamics methods, *J. Chem. Phys.* 81(1), 511 (1984)
50. W. G. Hoover, Canonical dynamics: Equilibrium phase-space distributions, *Phys. Rev. A* 31(3), 1695 (1985)
51. Z. X. Guo and X. G. Gong, Molecular dynamics studies on the thermal conductivity of single-walled carbon nanotubes, *Front. Phys. China* 4(3), 389 (2009)
52. I. C. Yeh and M. L. Berkowitz, Ewald summation for systems with slab geometry, *J. Chem. Phys.* 111(7), 3155 (1999)
53. C. K. Lo and K. W. Yu, Field-induced structure transformation in electrorheological solids, *Phys. Rev. E* 64(3), 031501 (2001)
54. J. P. Huang, J. T. K. Wan, C. K. Lo, and K. W. Yu, Nonlinear ac response of anisotropic composites, *Phys. Rev. E* 64(6), 061505 (2001)
55. G. Wang and J. P. Huang, Nonlinear magnetic susceptibility of ferrofluids, *Chem. Phys. Lett.* 421(4-6), 544 (2006)
56. L. D. Landau, E. M. Lifshitz, and L. P. Pitaevskii, Electrodynamics of Continuous Media, 2nd Ed., Pergamon, New York, 1984
57. C. Z. Fan and J. P. Huang, Second-harmonic generation with magnetic-field controllabilities, *Appl. Phys. Lett.* 89(14), 141906 (2006)
58. J. P. Huang and K. W. Yu, Enhanced nonlinear optical responses of materials: Composite effects, *Phys. Rep.* 431(3), 87 (2006)